metals

Article

Investigation on the Tensile Properties of Inconel 625 Using Small Punch Test

Changjian Li, Shuaichen Shi, Jianwen Zhang, Sisheng Yang * and Qingsheng Li

School of Mechanical and Power Engineering, Nanjing Tech University, Nanjing 211816, China
* Correspondence: sishengyang@njtech.edu.cn

Abstract: As a commonly used material in the petrochemical, nuclear and aerospace fields, Inconel 625 has excellent strength and corrosion resistance. The accurate evaluation of material properties with small specimen volume is of great significance to ensure in-service equipment safety. To realize reasonable estimations of tensile strength based on the small punch test, load–displacement and slope–displacement curves of Inconel 625 were discussed in this study. The results prove that the first inflexion point can be used in the yield strength analysis based on the empirical correlation method and plate bend theory. Meanwhile, the lowest point of the elastic and plastic deformation stages in the slope–displacement curves were compared. A new deformation energy method was established to realize yield strength estimations. To analyze the ultimate tensile strength, a small punch deformation feature was discussed based on the geometric deformation model and microstructure analysis. The relationship between stress and displacement was obtained. $F_m/d_m t_0$ was proven to be a more appropriate parameter in ultimate tensile strength estimations.

Keywords: small punch test; tensile properties; Inconel 625; empirical correlation; deformation energy

check for updates

Citation: Li, C.; Shi, S.; Zhang, J.; Yang, S.; Li, Q. Investigation on the Tensile Properties of Inconel 625 Using Small Punch Test. *Metals* **2024**, *14*, 411. https://doi.org/10.3390/met14040411

Academic Editor: Thomas Niendorf

Received: 29 February 2024
Revised: 25 March 2024
Accepted: 28 March 2024
Published: 29 March 2024

1. Introduction

Tensile properties of materials are fundamental parameters when estimating the strength degradation and structural integrity of practical facilities. In recent years, many works have been made to analyze material properties– based on miniaturized specimens [1,2]. Small material requirement means that miniature tests can be applied in mechanical properties analysis during the service lives of components. Meanwhile, they are applicable to degradation evaluations of uniform damage regions and local structures, such as welded joints and hydrogen embrittlement material [3]. Take the small punch test, for example, which permits a specimen thickness of about 0.5 mm [4]. The diameter of circular specimens or the side length of square specimens utilized is generally not greater than 10 mm [5]. Meanwhile, the feasibility of small punch analysis has been demonstrated in different temperature environments to obtain creep and low temperature strengths [6,7]. Due to this advantage, how to estimate material properties using the small punch test with small specimen volumes instead of traditional tests has attracted more and more attention.

Different to the stress–strain curve obtained from uniaxial tensile tests, the output of the small punch test is a load–displacement curve. Thus, small punch results should be further processed to realize materials properties' estimations [8,9]. The most widely used method is the empirical correlation method [10]. Based on the deformation feature and load–displacement curve analysis, a lot of empirical correlations have been established between small punch load parameters and tensile properties [11,12]. As shown in Figure 1, the initial slope of the elastic zone (S_e), yield load (F_y), maximum load (F_m) and the displacement corresponding to the maximum load (d_m) are obtained in load–displacement curves. The traditional empirical correlations can be expressed as follow [13,14]:

$$E = a_1 \frac{S_e}{t_0} \tag{1}$$

$$\sigma_y = a_2 \frac{F_y}{t_0^2} \tag{2}$$

$$\sigma_{ut} = a_3 \frac{F_m}{t_0^2} + a_4 \tag{3}$$

$$A = a_5 \frac{d_m}{t_0} \tag{4}$$

where E is the elastic modulus, σ_y is the yield strength, σ_{ut} is the ultimate tensile strength, A is the elongation, t_0 is the initial specimen thickness, and a_1, a_2, a_3, a_4 and a_5 are coefficients related to the material and fixture sizes. Yet, it is worth noting that the demarcation point of elastic deformation and plastic deformation phases is not obvious due to the non-uniform deformation characteristics. Thus, how to determine yield load has always been the focus of attention in previous studies. The crossing point of two tangents (or two fitted lines) of elastic and plastic stages was defined as yield load ($F_{y\text{-}Mao}$) [15]. The small punch load corresponding to the displacement of a crossing point has also been used ($F_{y\text{-}CEN}$) [16]. Some researchers drew a straight line parallel to the initial slope of the elastic region through a point at the x-axis such as $t_0/10$ and $t_0/100$. The crossing point of the small punch curve and straight line was defined as yield load ($F_{y\text{-}t/10}$ or $F_{y\text{-}t/100}$) [17]. Jose Calaf-Chica et al. pointed out that the influence of strain hardening should not be ignored in the traditional yield load analysis [18]. Thus, an optimized offset correlation method was proposed based on the minimum slope of the small punch plastic deformation region [19]. Different to yield load, the maximum load of a load–displacement curve is easy to determine. Thus, it is widely used in ultimate tensile strength analysis. Considering that the distribution of stress and strain is not uniform during the small punch deformation, Altstadt et al. believed that small punch load parameters at the onset of plastic instability were also suitable for estimating ultimate tensile strength [20].

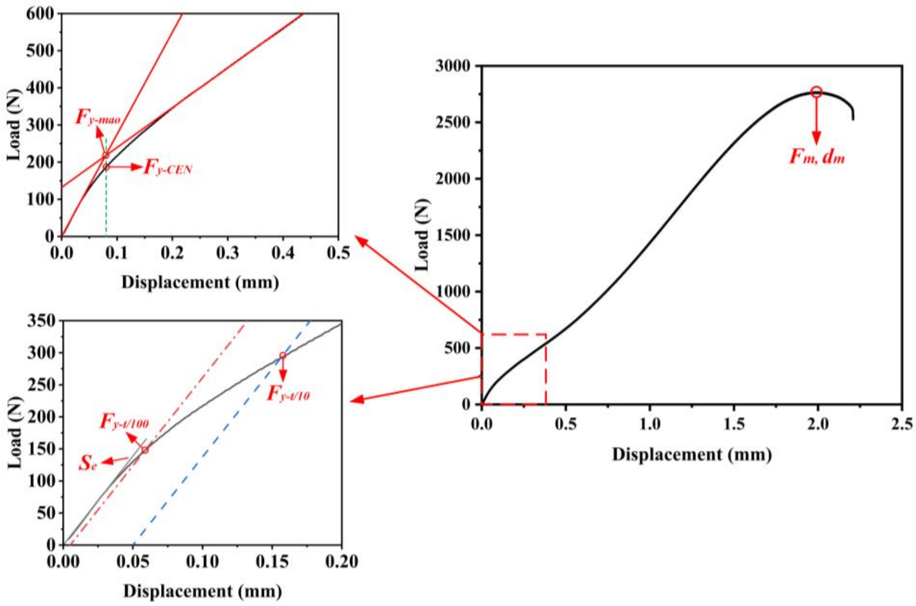

Figure 1. Small punch parameters obtained from load–displacement curve.

Based on the deformation feature analysis of small punch specimens, some direct calculation methods were also proposed in previous studies. Isselin and Shoji found that small punch elastic energy was proportional to the square of yield strength. Thus, an energy method was proposed based on the elastic energy determined by loading and unloading processes [21]. With the development of computer technology in recent years, finite element simulation has been gradually used in small punch deformation analyses and tensile properties prediction [22]. Husain et al. compared the experimental and simulation load–displacement curves to describe the constitutive materials behavior by inverse finite element procedures [23]. Pan et al. realized the prediction of Hollomon parameters and ultimate tensile strength by different machine learning models [24].

Compared with other methods, the advantages of the empirical correlation method are its simplicity and convenience. Thus, it has drawn lots of attention. However, as material changes, the fitting coefficients may change with it. The applicability of the fitting formula needs to be improved based on a large number of experimental data. As a typical nickel-based alloy, Inconel 625 is widely used in aerospace, petrochemical, nuclear power and other fields due to its excellent strength at high temperature and in corrosive environments. However, it is not clear whether previous relationships can be used in the tensile strength estimation of Inconel 625 directly. A similar issue is also found in machine learning. Data volume is a key role which can affect prediction accuracy. In this study, the load parameters and deformation energy of Inconel 625 were discussed. A tensile strength evaluation method based on the small punch test was established. The results may provide a reference for the in-service properties and fracture feature analysis of Inconel 625 in practical engineering.

2. Experimental

In this study, all experimental materials were taken from the same alloy plate with 12 mm in thickness. The microstructure of Inconel 625 used here is shown in Figure 2. The geometrical shape and size of the specimens are shown in Figure 3. It is easy to find that the volume and size of a small punch specimen is far smaller than that of traditional tensile specimens. Before the test, the surfaces of small punch and tensile specimens were sanded by abrasive papers with various degrees of roughness firstly. When the specimen thickness was close to the set value, the surfaces were further polished by metallographic sandpaper to avoid surface effects.

Figure 2. Microstructure of Inconel 625.

Because of the small thickness, size effect can not be neglected in the small punch analysis. Thus, several small punch specimens with different thicknesses from 0.4 mm to 0.65 mm were used here. The schematic diagram of a self-designed small punch fixture is shown in Figure 4. The diameter of the lower die hole was 4 mm. In the experimental preparation process, the specimen was clamped between the upper die and lower die. Then, the fixture was installed on an Instron 5869 universal testing machine. During the test, the load was transferred onto the specimen by a hemispherical punch that was 2.4 mm in diameter. Along with the increase in deformation, load and displacement data were recorded up to failure, which was indicated by an obvious drop in the load. In addition to the small punch fracture test, interrupted test was also completed here to obtain the small punch deformation feature at different displacements. Finally, the interrupted and failure specimens were cut along the center line and observed by a scanning electron microscope.

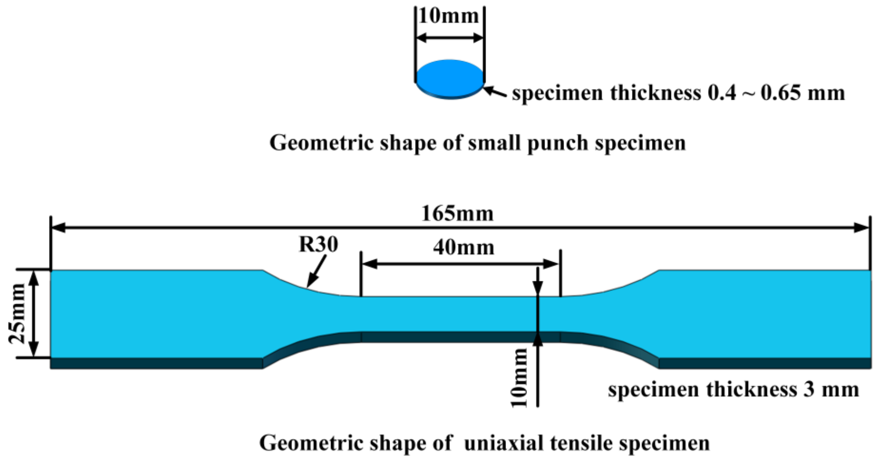

Figure 3. Schematic diagram of small punch specimen and uniaxial tensile specimen.

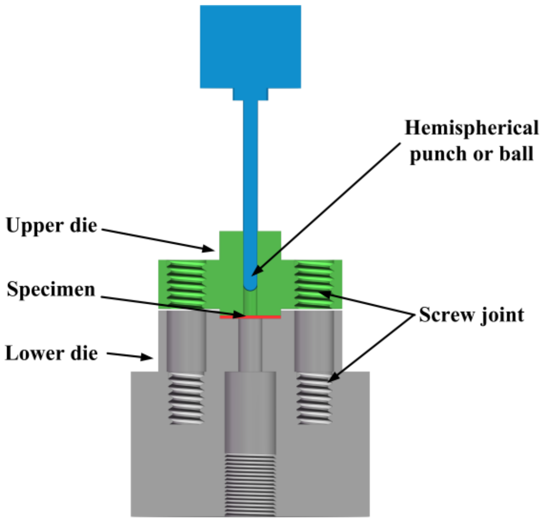

Figure 4. Schematic diagram of small punch fixture.

To obtain the tensile properties of Inconel 625 and verify the analysis results of the small punch test, tensile tests were also completed on the Instron 5869 universal testing machine. As described above, the specimens were polished to ensure that the thickness in the gauge length was uniform. Then, one side of the tensile specimen was fixed and the other side was stretched. An extensometer was used to measure the strain in the stretching direction and obtain the stress–strain curves. The tensile rate of the uniaxial specimen was 1 mm/min. Meanwhile, three displacement rates (0.05 mm/min, 0.25 mm/min and 0.5 mm/min) were selected in the small punch test to discuss the effect of the deformation rate on the tensile strength estimation method.

3. Tensile Strength Estimation Based on Characteristic Load

3.1. Yield Strength Estimation Based on the First Inflection Point

The small punch and uniaxial tensile results of Inconel 625 are shown in Figure 5. In the initial stage, elastic deformation is produced during the contact process of the specimen and the punch. Similar to the stress–strain curves, the load–displacement curve is also a straight line at this stage. Thus, this stage is widely defined as the elastic deformation stage. With the increase in deformation, plastic deformation occurs in different areas. The slope of the load–displacement curve changes gradually in this stage. The remarkable thing is that the yield platform cannot be found in the small punch curve even if the uniaxial tensile curve has this characteristic. Then, the small punch deformation enters the membrane stretching stage with the increase in displacement. Different to the hardening stage of the uniaxial tensile curve, the membrane stretching stage of the load–displacement curves is an approximate line. It is hard to calculate the strain hardening parameters directly based on small punch characteristic parameters using the empirical correlation method. On approaching the highest point, the slope decreases gradually. At this stage, a crack grows along with apparent necking phenomenon. Finally, failure of specimen happens when the small punch load declines from the maximum value. It should be noted that the rate of decline may change with thickness and material characteristics. For ductile material such as Inconel 625, the rate of decline may be slower. Meanwhile, an apparent arc is presented in the fracture stage.

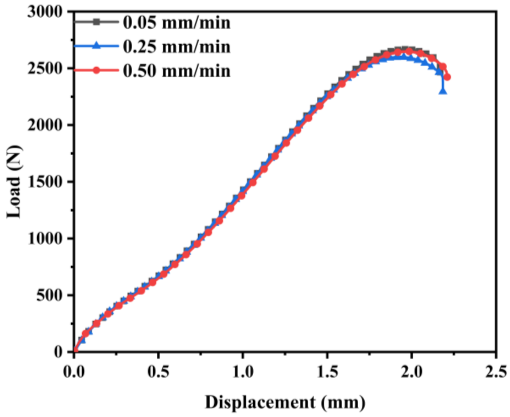

(**a**)

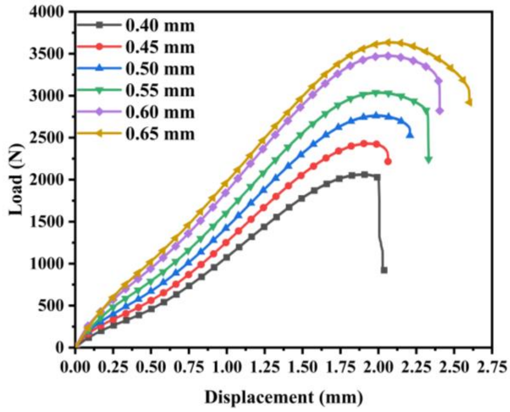

(**b**)

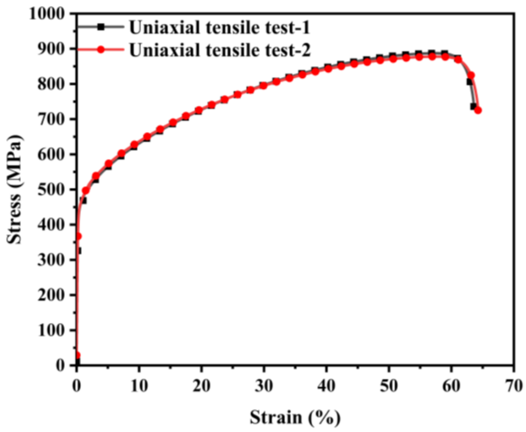

(**c**)

Figure 5. Small punch and uniaxial tensile results of Inconel 625 (**a**) load–displacement curves with different displacement rates, (**b**) load–displacement curves with different specimen thicknesses at 0.5 mm/min, (**c**) stress-strain curves.

To estimate the tensile strengths of Inconel 625 reasonably, load–displacement curves were studied via variations in the deformation rate at room temperature as shown in Figure 5a. The results indicate that the load–displacement curves with different deformation rates have a high consistency. This means that there is not an apparent strain rate sensitivity during the small punch deformation of Inconel 625 at room temperature. The small punch displacement rate does not play an important role in the tensile strength estimation of Inconel 625 in this study. On the other hand, small punch tests with different specimen thicknesses were completed at 0.5 mm/min and are shown in Figure 5b. Different to the deformation rate, thickness is a key factor that cannot be neglected in the tensile strength analysis [25]. With the increase in specimen thickness, larger small punch parameters were obtained along with a higher curve. To describe the influence of specimen thickness clearer, small punch characteristic parameters obtained in the load–displacement curves were compared here. The evolutions of $F_{y\text{-}CEN}$, $F_{y\text{-}t/100}$ and $F_{y\text{-}i}$ along with the change in thickness are shown in Figure 6a. Different to $F_{y\text{-}CEN}$ and $F_{y\text{-}t/100}$, $F_{y\text{-}i}$ is the load corresponding to the first inflexion point obtained in the elastic deformation stage. Thus, the advantage of the first inflexion method is that it is less affected by strain hardening parameters.

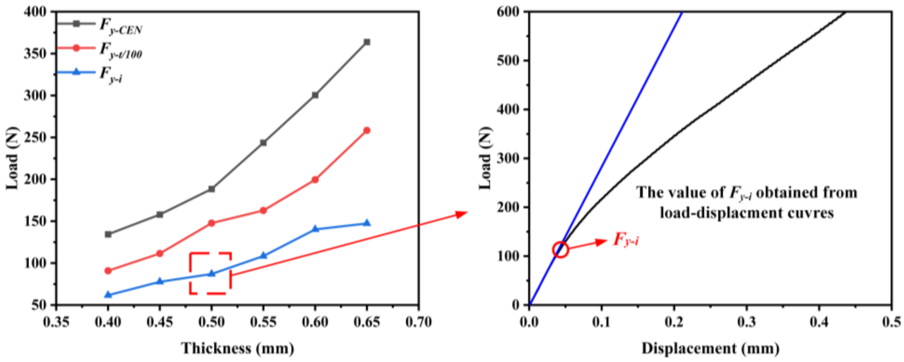

(**a**)

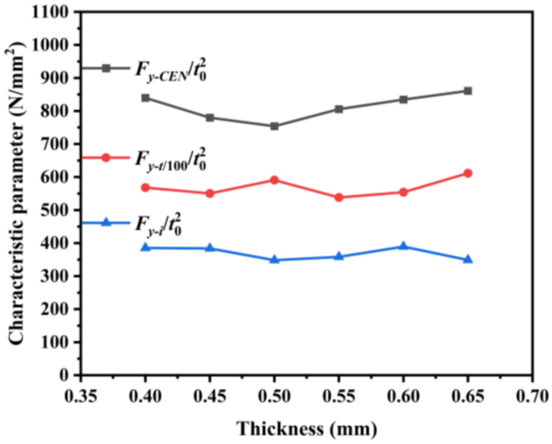

(**b**)

Figure 6. The relationship between small punch characteristic parameters and specimen thickness (**a**) $F_{y\text{-}CEN}$, $F_{y\text{-}t/100}$ and $F_{y\text{-}i}$, (**b**) $F_{y\text{-}CEN}/t_0^2$, $F_{y\text{-}t/100}/t_0^2$ and $F_{y\text{-}i}/t_0^2$.

As shown in Figure 6a, the yield load increases with increasing specimen thickness. This is because this yielding process first happens in the upper surface [26]. With the increase in the small punch displacement, the yield area grows. A larger load is needed to make the lower surface of the specimen yield when specimen thickness increases. Considering the influence of specimen thickness, $F_{y\text{-}CEN}/t_0^2$, $F_{y\text{-}t/100}/t_0^2$ and $F_{y\text{-}i}/t_0^2$ are compared in Figure 6b. It can be found that there is not a significant change in $F_{y\text{-}CEN}/t_0^2$, $F_{y\text{-}t/100}/t_0^2$ and $F_{y\text{-}i}/t_0^2$ with increasing thickness. The ratio of yield load and initial specimen thickness is an approximate constant. This means that the ratio of yield load and the square of the initial specimen thickness can be used to estimate the yield strength of Inconel 625 based on the empirical correlation method.

The other notable thing is that the there is a significant difference between the yield loads obtained by different methods. This is because that small punch deformation is a non-uniform process. The stress at different deformation regions will not reach yield values at the same time. This is also one reason that part of the small punch yield load cannot be used in theoretical models to calculate yield strength directly. José Calaf Chica et al. indicated that yielded areas could be found in the specimen center under punch firstly in the elastic deformation region [26]. When the yield area grows from the upper surface to the lower surface along the thickness direction, a complete yielded area in the specimen center is found. It is important to note that the corresponding location is close to the first inflection point. Meanwhile, the parameters at the corresponding displacement are mainly related to yield strength and less affected by strain hardening parameters. Thus, the first inflection point in the load–displacement curve may be an appropriate parameter used in yield strength calculations based on empirical correlation and direct calculation methods. To test the idea, the plate bend theory is used here. In the elastic deformation region, the variation in specimen thickness is not obvious. Thus, the thickness is assumed to be a constant and uniform. On the basis of the geometrical shape of the flat circular plate, the relationship between the equivalent contact radius and displacement can be described as follows:

$$r'^2 + (r-d)^2 = r^2 \tag{5}$$

where d is the displacement, r is the ball radius, and r' is the equivalent contact radius. Then, the equivalent contact radius can further be obtained:

$$r' = \sqrt{2rd - d^2} \tag{6}$$

The yield strength calculated by the small punch load is expressed as follows [27]:

$$\sigma_y = \frac{3F_{y-i}(1+\nu)}{2\pi t_0^2} \ln \frac{R}{r'} \tag{7}$$

where R is the lower hole radius, and ν is the Poisson ratio.

Equation (7) shows that the yield strength is proportional to the yield load, which is also the basis of previous empirical correlation analyses. Based on Equations (6) and (7), $F_{y\text{-}i}/t_0^2$ was used to calculate the yield strength. The small punch calculated results and uniaxial tensile results are shown in Figure 7. It is shown that there is a high consistency between the tensile result and calculated value based on the plate bend theory, which indicates that the yield load at the first inflection point is suitable to estimate the yield strength of Inconel 625.

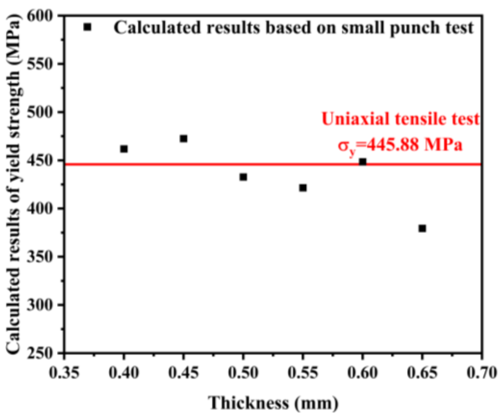

Figure 7. Calculated results of yield strength based on plate bend theory.

3.2. Ultimate Tensile Strength Estimation Based on the Maximum Load

The maximum stress of the stress–strain curve is defined as the ultimate tensile strength of material. Thus, the maximum load at the load–displacement curve is widely used to estimate the ultimate tensile strength in small punch analysis. As shown in Figure 5b, an apparent increase in the maximum load is presented with increasing specimen thickness. A simple linear relationship between $F_m/F_{m\text{-}0.5}$ and specimen thickness is obtained and expressed as follows:

$$F_m/F_{m\text{-}0.5} = 2.33t_0 - 0.174 \tag{8}$$

where $F_{m\text{-}0.5}$ is the maximum load when the specimen thickness is 0.5 mm. Another concern is the thickness variation. The deformation feature of small punch specimens at different displacements is observed by a scanning electron microscope and shown in Figure 8. An apparent thickness reduction is presented due to large deformations in the membrane stretching and instability stage. Meanwhile, the necking phenomenon can also be found at the contact boundary. Finally, failure will happen in this region along with apparent ductile fracture characteristics. The ductile fracture feature can also be found in the uniaxial tensile results [28], which proves that the small punch test can be used to estimate the tensile strength of Inconel 625.

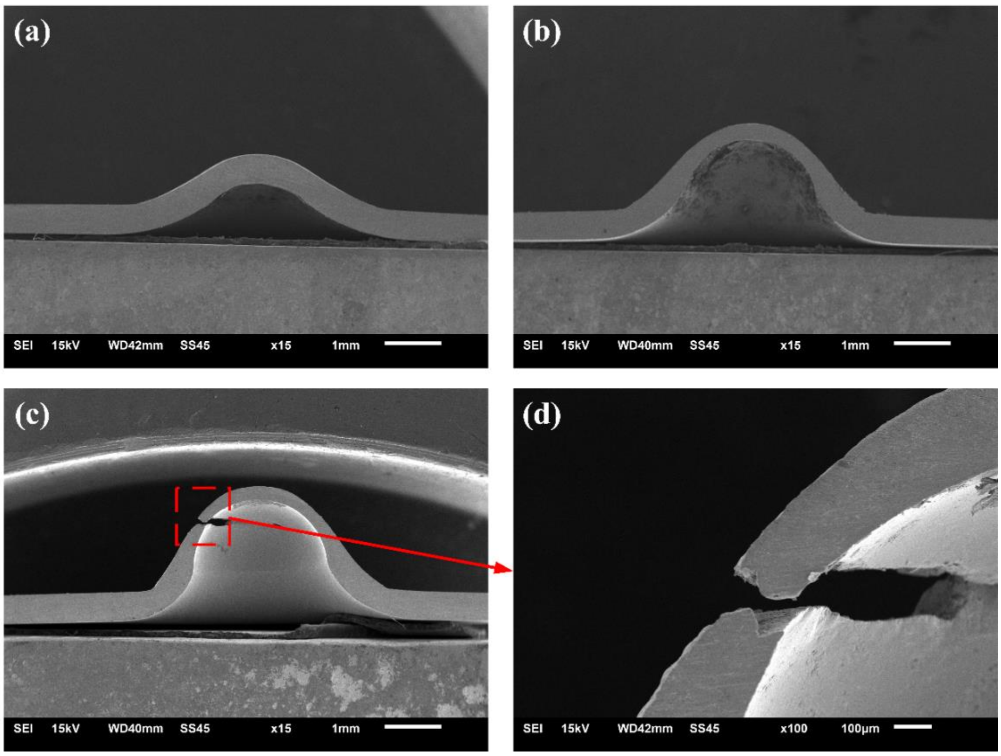

Figure 8. Small punch deformation features at different displacements (**a**) in the membrane stretching stage (**b**) at maximum load point, (**c**) failure specimen, (**d**) fracture morphology.

Due to the cone feature in the non-contact region, Hyde et al. derived the relationship between current thickness t and deformation angle α based on the constant volume assumption [29]:

$$t = t_0/\sqrt{1 + 1/\tan^2\alpha} \tag{9}$$

As shown in Figure 9a, the maximum stress σ_m at the contact boundary is calculated as follows:

$$\sigma_m = \frac{F}{2\pi r t_0 \cos\alpha}\frac{\sqrt{1 + 1/\tan^2\alpha}}{\cos\alpha} \tag{10}$$

In Equation (10), F is the load. The value of α decreases with the increase in displacement:

$$d = \frac{R}{\tan\alpha} - \frac{r}{\sin\alpha} + r \tag{11}$$

Based on Equations (10) and (11), the variations in $\sqrt{1+1/\tan^2\alpha}/\cos^2\alpha$ can be described as shown in Figure 9b. An approximate linear relationship can be found between $\sqrt{1+1/\tan^2\alpha}/\cos^2\alpha$ and the reciprocal of the maximum displacements along with the change in specimen thickness. The small deviation is because of the assumption that uniform thickness is not suitable in the failure stage due to the necking phenomenon. As a whole, it is seen that that small punch stress is inversely proportional to the displacement and initial specimen thickness. Thus, the initial specimen thickness and displacement corresponding to the maximum load should be considered in the ultimate tensile analysis of Inconel 625. With the increase in the initial specimen thickness, a larger specimen thickness at the maximum load point is found. Considering the consistency of the unit of strength and small punch characteristic parameters [30], $F_m/d_m t_0$ and $F_m/{t_0}^2$ are used, and the results are shown in Figure 10.

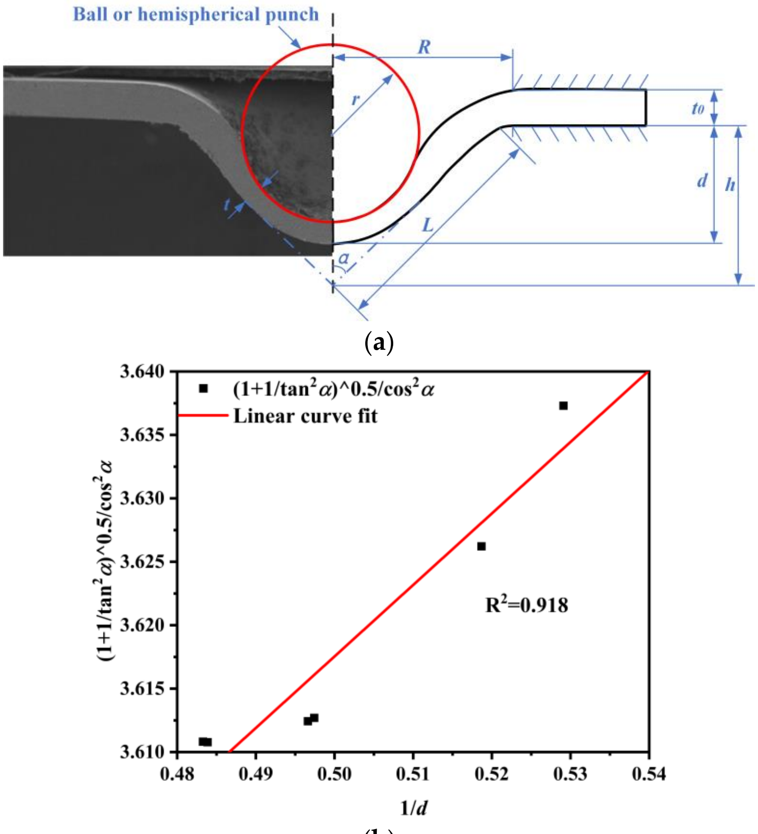

(**a**)

(**b**)

Figure 9. Small punch deformation analysis. (**a**) Small punch geometric deformation model. (**b**) The relationship between $\sqrt{1+1/\tan^2\alpha}/\cos^2\alpha$ and $1/d$.

It can be found that $F_m/d_m t_0$ is an approximate constant with the increase in specimen thickness. By comparison, the apparent change in $F_m/{t_0}^2$ is shown in Figure 10, which proves that $F_m/d_m t_0$ is a more suitable choice. In this study, small punch results with four specimen thicknesses (0.4 mm, 0.45 mm, 0.5 mm, 0.55 mm) were used to establish the relationship between the ultimate tensile strength and $F_m/d_m t_0$. The fitted result is shown in Equation (12).

$$\sigma_{ut} = 0.318\frac{F_m}{d_m t_0} \tag{12}$$

Based on Equation (12), the ultimate tensile strength of Inconel 625 can be predicted by the small punch maximum load and the corresponding displacement. The predicted results of other small punch results are 892.54 MPa (0.6 mm in thickness) and 860.02 MPa (0.65 mm in thickness). Compared to the ultimate tensile strength obtained by the uniaxial tensile test (878 MPa), the error is small. Meanwhile, Equation (12) is also used to estimate the ultimate tensile strength of Inconel 617 based on our previous experimental results [31]. The predicted value of the small punch results is 843.05 MPa, and the uniaxial tensile result is 816.67 MPa. It can be found that $F_m/d_m t_0$ is an appropriate parameter to estimate the ultimate tensile strength of a nickel-based alloy at room temperature.

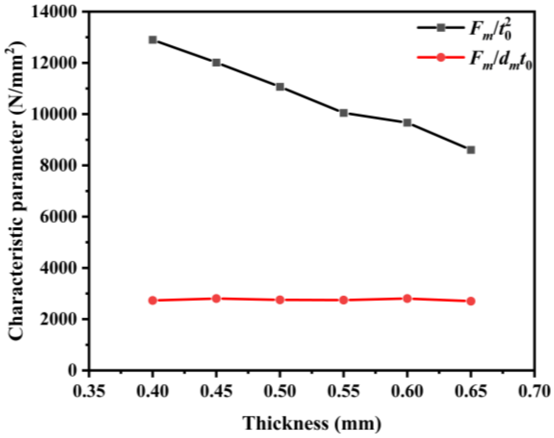

Figure 10. The influence of specimen thickness on $F_m/d_m t_0$ and $F_m/{t_0}^2$.

4. Yield Strength Analysis Based on Deformation Energy

As small punch deformation increases, the area under the load–displacement curve increases, and a larger deformation energy is obtained. An attempt was made by Singh et al. to analyze the mechanical strength of Cr–Mo grade steel based on energy parameters [32]. The deformation energy calculated by area was proven to be closely related to the mechanical work acting on the specimen and has the potential to estimate material strength in small punch analysis. Compared to the load method, energy parameters were less affected by experimental errors such as the small change in the elastic and plastic deformation curves. However, the yield load point determined by the load method was also used in the previous research to calculate small punch deformation energy parameters. The deviation in the yield load analysis will also affect the accuracy of deformation energy evaluations. To overcome this, a new deformation energy estimated method is proposed in this section.

In this study, the load–displacement curves are divided into many intervals to calculate the slope. Each interval contains about fifty data points to avoid the influence of individual discrete data. When the slope changes rapidly, less data points are contained to guarantee that the load–displacement curve is an approximate line in this interval. The analysis result is shown in Figure 11. As a function of displacement, Pandey et al. found that the slope of load–displacements curve can be divided into four different deformation regions affected by mechanical behavior [33]. It can be found that a linear decrement appears in the elastic deformation stage. With the increase in small punch displacement, the descent rate slows down and an arc curve is presented due to the non-uniform deformation feature. As the curve enters the plastic deformation stage, the material in the center zone has yielded. Meanwhile, part of the material not in specimen center is still in the elastic deformation stage. The lowest point of the elastic and plastic deformation stages in the slope–displacement curve is obtained. Most of the material in the contact region has yielded at this time. Beyond this stage, the slope–displacement curve rises slowly along with the influence of strain hardening and uniform thickness reduction. When thickness reduction dominates the deformation process, the curve decreases again and reaches zero at the displacement corresponding to the maximum load of the load–displacement curve. This also proves that the load at this point can be used in ultimate tensile estimations as discussed in the previous section.

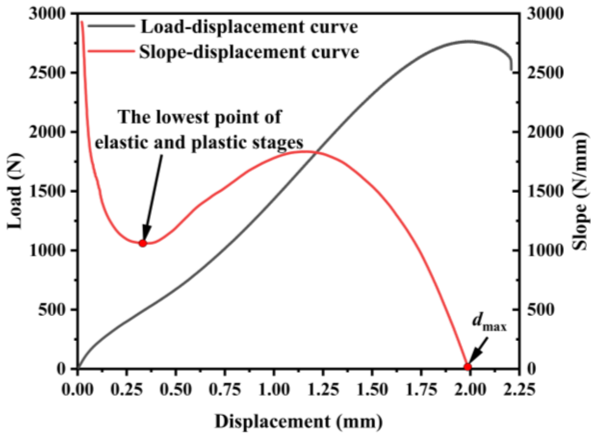

Figure 11. Comparison of load–displacement and slope–displacement curves.

To investigate the influence of specimen thickness, the slope–displacement curves of Inconel 625 with different thicknesses were studied and are shown in Figure 12. The results indicate that a higher slope–displacement curve is obtained with the increase in specimen thickness. Meanwhile, the displacement corresponding to the zero point increases, as shown in Figure 13. This is because more mechanical work is needed to make material yield when thickness increases. Thus, the lowest point of the elastic and plastic deformation stages in the slope–displacement curves was found to be an approximate parameter to estimate the yield strength of Inconel 625. To verify the conclusion, the deformation energy corresponding to this point (E_y) was calculated and is shown in Figure 14a. It is observed that the deformation energy increases with the increase in specimen thickness. To eliminate the influence of specimen thickness, the evolution of $E_y/d_y{t_0}^2$ was analyzed and is shown in Figure 14b. d_y is the displacement corresponding to the lowest point in the elastic and plastic deformation stages. It can be found that there is no apparent change in deformation energy parameters along with the variation in thickness. Thus, yield strength and small punch deformation energy parameters with four specimen thicknesses (0.4 mm, 0.45 mm, 0.5 mm, 0.55 mm) were fitted and are listed here:

$$\sigma_y = 0.391\frac{E_y}{d_y t_0^2} \tag{13}$$

Based on Equation (13), the calculated results of other small punch deformation energy parameters are 498.90 MPa (specimen thickness is 0.6 mm) and 474.07 MPa (specimen thickness is 0.65 mm). The yield strength obtained by the uniaxial tensile test is 445.88 MPa. Meanwhile, Equation (13) is also used to calculate the yield strength of Inconel 617. The small punch calculated result is 438.44 MPa and the uniaxial tensile result is 403.97 MPa [31]. It can be found that the prediction accuracy of yield strength is lower than that of ultimate tensile strength as discussed in the previous section. This is because the material of the small punch specimen will not enter the plastic deformation stage simultaneously. As a whole, $E_y/d_y{t_0}^2$ can be used in the yield strength analysis of Inconel 625 considering the influence of geometrical size.

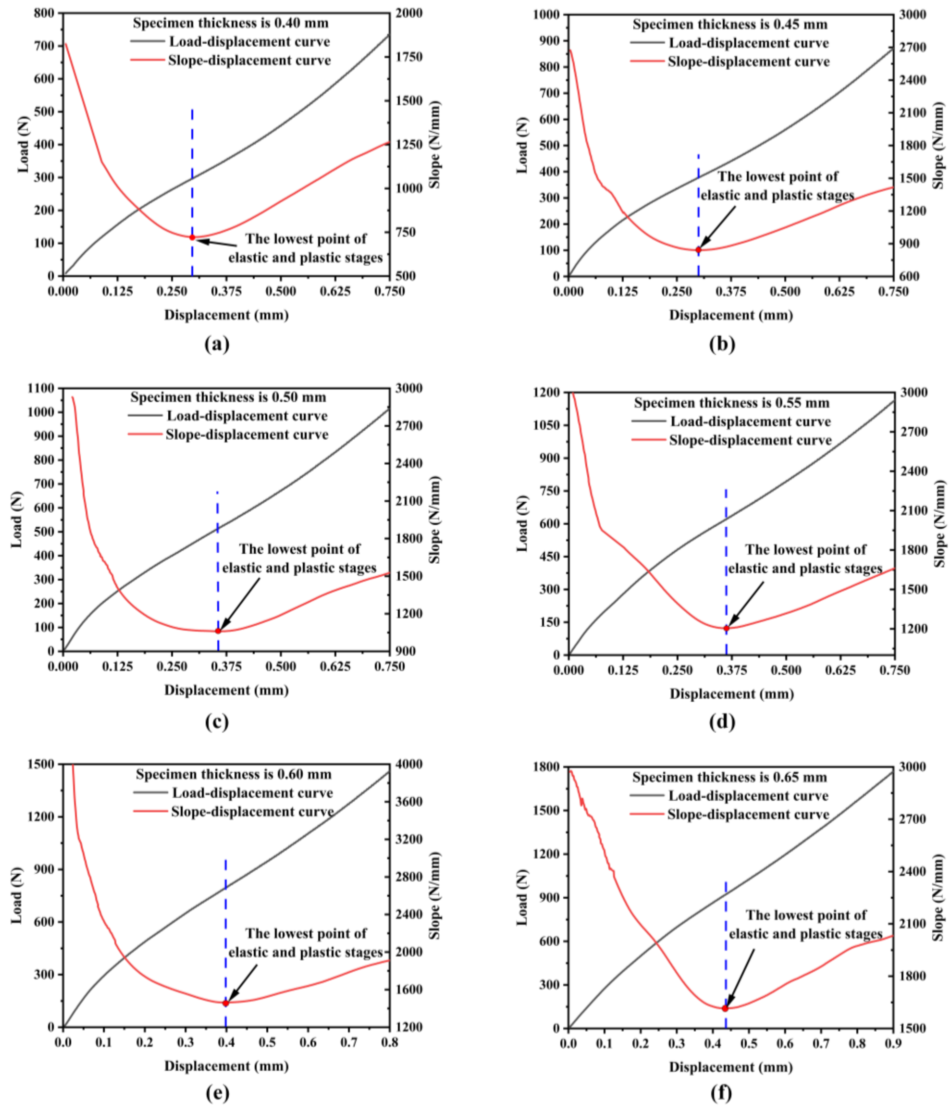

Figure 12. The influence of specimen thickness on the lowest point of elastic and plastic deformation stages, (**a**) 0.4 mm, (**b**) 0.45 mm, (**c**) 0.5 mm, (**d**) 0.55 mm, (**e**) 0.6 mm, (**f**) 0.65 mm.

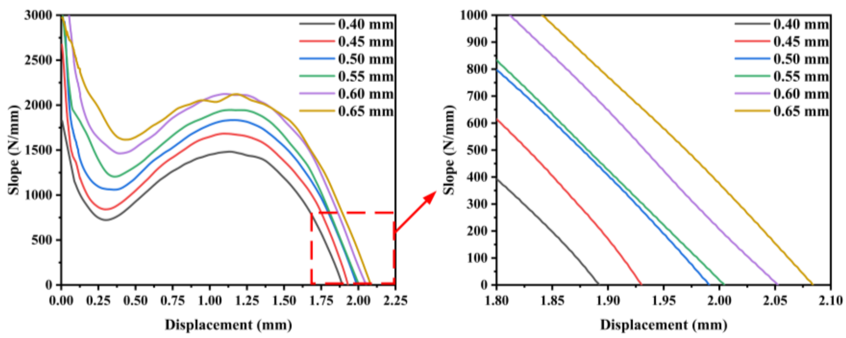

Figure 13. Zero points of slope–displacement curves.

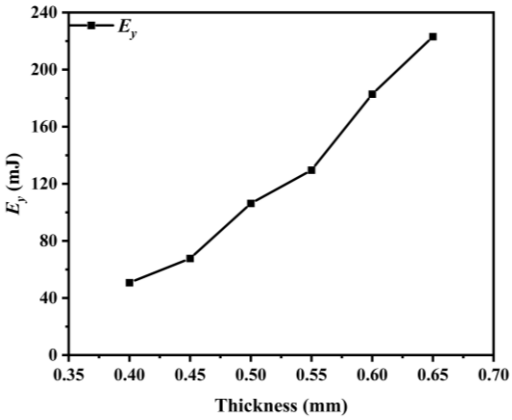

(**a**)

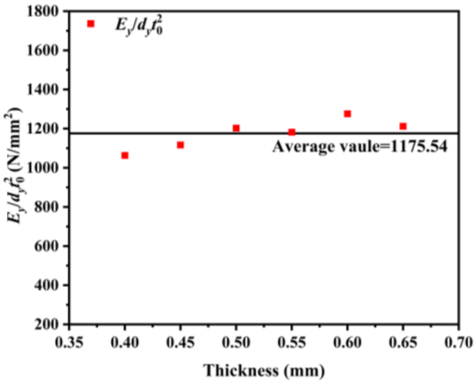

(**b**)

Figure 14. The change in deformation energy parameters along with the increase in specimen thickness (**a**) E_y, (**b**) $E_y/d_yt_0{}^2$.

5. Conclusions

Compared to the uniaxial tensile test, the small punch test is a more appropriate choice in the tensile strength analysis of in-service structure due to the small specimen size. In this study, the small punch test and the uniaxial tensile test of Inconel 625 were completed. The influence of specimen thickness and the displacement rate was discussed. Different tensile strength estimated methods were established. The following conclusions were drawn:

(1) The first inflection load obtained in the load–displacement curve is a suitable parameter to calculate the yield strength of Inconel 625 based on the empirical correlation method and plate bend theory.

(2) The maximum stress is found to be proportional to the maximum load and inversely proportional to maximum load–displacement based on the geometric deformation model analysis. F_m/d_mt_0 is an appropriate parameter in the ultimate tensile strength analysis.

(3) A new yield strength estimation method based on the small punch deformation energy parameter and slope–displacement curve is established.

Author Contributions: Conceptualization, C.L. and S.Y.; data curation, S.Y.; formal analysis, C.L. and S.S.; funding acquisition, Q.L.; investigation, C.L. and J.Z.; methodology, C.L., S.S., J.Z. and S.Y.; supervision, S.Y.; validation, S.S. and S.Y.; writing—original draft, C.L.; writing—review and editing, S.S., J.Z., S.Y. and Q.L. All authors have read and agreed to the published version of the manuscript.

Funding: This research is funded by the National Key Research and Development Program of China (Grant No. 2018YFA0704604).

Data Availability Statement: The data presented in this study are available on request from the corresponding author.

Conflicts of Interest: The authors declare no conflict of interest.

References

1. Fleury, E.; Ha, J.S. Small punch tests to estimate the mechanical properties of steels for steam power plant: I. Mechanical strength. *Int. J. Press. Ves. Pip.* **1998**, *75*, 699–706. [CrossRef]
2. Tian, X.; Zhang, S.F.; Xu, H.; Li, T.J.; Yang, B.X.; Zhang, M. Assessment of Creep Properties Using Small Punch Test for a 9%Cr-Mo-Co-B Power Plant Steel. *Metals* **2021**, *11*, 1996. [CrossRef]
3. Nguyen, T.T.; Park, J.; Bae, K.-O.; Baek, U.B. Correlation between in-situ small punch and conventional test result in evaluating hydrogen embrittlement susceptibility of API X70 base and weld under hydrogen gas mixture. *Eng. Fail. Anal.* **2024**, *159*, 108047. [CrossRef]
4. Milička, K.; Dobes, F. Small punch testing of P91 steel. *Int. J. Press. Ves. Pip.* **2006**, *83*, 625–634. [CrossRef]
5. García, T.E.; Rodríguez, C.; Belzunce, F.J.; Cuesta, I.I. Effect of hydrogen embrittlement on the tensile properties of CrMoV steels by means of the small punch test. *Mat. Sci. Eng. A* **2016**, *664*, 165–176. [CrossRef]
6. Nguyen, T.T.; Yoon, K.B. Fully plastic J-integral and C* equations for small punch test specimen with a surface crack. *Int. J. Press. Ves. Pip.* **2020**, *188*, 104214. [CrossRef]
7. Altstadt, E.; Bergner, F.; Houska, M. Use of the small punch test for the estimation of ductile-to-brittle transition temperature shift of irradiated steels. *Nucl. Mater. Energy* **2021**, *26*, 100918. [CrossRef]
8. Hähner, P.; Soyarslan, C.; Çakan, B.G.; Bargmann, S. Determining tensile yield stresses from Small Punch tests: A numerical-based scheme. *Mater. Design* **2019**, *182*, 107974. [CrossRef]
9. Melkior, T.; Terentyev, D.; Chang, C.C.; Bakaev, A.; Holmström, S.; Lebediev, S.; Paputsia, A. Mechanical properties of structural metallic alloys for nuclear applications deduced by small punch test. *J. Nucl. Mater.* **2023**, *583*, 154521. [CrossRef]
10. Mahalle, G.; Davis, T.P.; Lee, W.E.; Mamun, A.A. Investigation of strain-rate sensitivity of T91 Steel Using Small Punch Testing. *Procedia Struct. Integr.* **2022**, *42*, 570–577. [CrossRef]
11. *BS EN 10371: 2021*; Metallic Materials-Small Pinch Test Method. CEN: Brussels, Belgium, 2021.
12. *ASTM E3205-20*; Standard Test Method for Small Punch Testing of Metallic Materials. ASTM: West Conshohocken, PA, USA, 2020.
13. Calaf-Chica, J.; Bravo Díez, P.M.; Preciado Calzada, M. Improved correlation for elastic modulus prediction of metallic materials in the Small Punch Test. *Int. J. Mech. Sci.* **2017**, *134*, 112–122. [CrossRef]
14. Janča, A.; Siegl, J.; Haušild, P. Small punch test evaluation methods for material characterization. *J. Nucl. Mater.* **2016**, *481*, 201–213. [CrossRef]
15. Mao, X.; Takahashi, H. Development of a further-miniaturized specimen of 3 mm diameter for TJZM disk (0.3 mm) small punch tests. *J. Nucl. Mater.* **1987**, *150*, 42–52. [CrossRef]
16. Leclerc, N.; Khosravani, A.; Hashemi, S.; Miracle, D.B.; Kalidindi, S.R. Correlation of measured load-displacement curves in small punch test with tensile stress-strain curves. *Acta Mater.* **2021**, *204*, 116501. [CrossRef]
17. Rodríguez, C.; Cabezas, J.G.; Cárdenas, E.; Belzunce, F.J.; Betegón, C. Mechanical properties characterization of heat-affected zone using the small punch test. *Weld. J.* **2009**, *88*, 188–192.
18. Calaf-Chica, J.; Bravo Díez, P.M.; Preciado Calzada, M.; Ballorca-Juez, D. A systematic FEM analysis of the influence of mechanical properties in the reliability of the correlation methods in the small punch test. *Int. J. Mech. Sci.* **2019**, *153–154*, 299–309. [CrossRef]
19. Calaf-Chica, J.; Bravo Díez, P.M.; Preciado Calzada, M.; Garcia-Tarrago, M.-J. Optimization of the t/10 offset correlation method to obtain the yield strength with the Small Punch Test. *J. Nucl. Mater.* **2020**, *534*, 152177. [CrossRef]
20. Altstadt, E.; Houska, M.; Simonovski, I.; Bruchhausen, M.; Holmström, S.; Lacalle, R. On the estimation of ultimate tensile stress from small punch testing. *Int. J. Mech. Sci.* **2018**, *136*, 85–93. [CrossRef]
21. Isselin, J.; Shoji, T. Yield strength evaluation by small-punch test. *J. Test. Eval.* **2009**, *37*, 531–537. [CrossRef]
22. Abendroth, M.; Kuna, M. Identification of ductile damage and fracture parameters from the small punch test using neural networks. *Eng. Fract. Mech.* **2006**, *73*, 710–725. [CrossRef]
23. Husain, A.; Sehgal, D.K.; Pandey, R.K. An inverse finite element procedure for the determination of constitutive tensile behavior of materials using miniature specimen. *Comp. Mater. Sci.* **2004**, *31*, 84–92. [CrossRef]
24. Pan, H.Y.; Peng, J.; Geng, X.X.; Gao, M.X.; Miao, X.T. Prediction of mechanical properties for typical pressure vessel steels by small punch test combined with machine learning. *Int. J. Press. Ves. Pip.* **2023**, *206*, 105060. [CrossRef]
25. Moreno, M.F. Effects of thickness specimen on the evaluation of relationship between tensile properties and small punch testing parameters in metallic materials. *Mater. Des.* **2018**, *157*, 512–522. [CrossRef]
26. Calaf-Chica, J.; Bravo Díez, P.M.; Preciado Calzada, M. Development of an improved prediction method for the yield strength of steel alloys in the Small Punch Test. *Mater. Des.* **2018**, *148*, 153–166. [CrossRef]
27. Mak, J.; Wei, T.; Wuhrer, R.; Yeung, W.; Heness, G.; Di, Z. A Solution for Estimating the Tensile Yield Strength from Small Specimens. *J. Test. Eval.* **2013**, *41*, 647–650. [CrossRef]
28. Anand Badrish, C.; Kotkunde, N.; Mahalle, G.; Singh, S.K.; Mahesh, K. Analysis of hot anisotropic tensile flow stress and strain hardening behavior for Inconel 625 alloy. *J. Mater. Eng. Perform.* **2019**, *28*, 7537–7553. [CrossRef]
29. Hyde, T.H.; Stoyanov, M.; Sun, W.; Hyde, C.J. On the interpretation of results from small punch creep tests. *J. Strain. Anal. Eng.* **2010**, *45*, 141–164. [CrossRef]
30. García, T.E.; Rodríguez, C.; Belzunce, F.J.; Suárez, C. Estimation of the mechanical properties of metallic materials by means of the small punch test. *J. Alloys Compd.* **2014**, *582*, 708–717. [CrossRef]

31. Yang, S.S.; Xue, L.; Lu, W.B.; Ling, X. Experimental study on the mechanical strength and dynamic strain aging of Inconel 617 using small punch test. *J. Alloys Compd.* **2020**, *815*, 152447. [CrossRef]
32. Singh, S.P.; Bhattacharya, S.; Sehgal, D.K. Evaluation of high temperature mechanical strength of Cr–Mo grade steel through small punch test technique. *Eng. Fail. Anal.* **2014**, *39*, 207–220. [CrossRef]
33. Pandey, A.V.; Karthik, V.; Shaik, A.R.; Kolhatkar, A.; Divakar, R. Estimation of UTS from small punch test using an Improved method. *Int. J. Press. Ves. Pip.* **2022**, *200*, 104818. [CrossRef]